PRAMANA — journal of physics

© Indian Academy of Sciences

Vol. 84, No. 5
May 2015
pp. 861–880

Electromagnetic probes of strongly interacting matter

JAN-E ALAM

Theoretical Physics Division, Variable Energy Cyclotron Centre, 1/AF, Bidhan Nagar, Kolkata 700 064, India
E-mail: jane@vecc.gov.in

DOI: 10.1007/s12043-015-0978-8; ***e*Publication:** 7 May 2015

Abstract. The nuclear matter under extreme conditions of temperatures (T) and baryonic densities (n_B) undergoes a phase transition to quark gluon plasma (QGP). It is expected that such extreme conditions can be achieved by colliding nuclei at ultrarelativistic energies. In the present review, the suitability of photons and dileptons as diagnostic tools of QGP has been discussed. The photon and dilepton spectra originating from heavy-ion collisions at LHC energies have been explicitly displayed in this article. Results from SPS and RHIC have been discussed adequately with appropriate references. The role of single electron spectra originating from the decays of heavy flavoured mesons on QGP detection has also been discussed briefly.

Keywords. Hadrons, quark gluon plasma; photons; dileptons; heavy flavours; hydrodynamic flow.

PACS Nos 25.75.−q; 25.75.Dw; 24.85.+p

1. Introduction

The theory of strong interaction, the quantum choromodynamics (QCD) predicts that at temperatures ∼170 MeV and baryon densities ∼(5−10)×normal nuclear matter density, hadrons melt down to a new phase of matter called quark gluon plasma (QGP) [1]. In the QGP, the quarks are not confined within a typical hadronic dimension but roam in a volume of nuclear dimension. According to the Big Bang model of cosmology, the microsecond old Universe has undergone a transition from QGP to hadrons. This transition assumes special importance because: (i) contrary to others (GUT, electroweak etc.) the QCD transition in the early Universe is the only one which can be achieved in the laboratory and (ii) while the 2.7 K microwave background radiation does not provide information about the Universe for time not earlier than 300,000 years after the Big Bang, the access to quark–hadron (q–h) phase transition will provide information on the state of the Universe when it was a few microsecond old. Therefore, the understanding of the early Universe compels us to study the q–h transition in the laboratory. It is expected that such a transition can be created in the laboratory by colliding two nuclei at ultrarelativistic energies. The Brookhaven National Laboratory's Relativistic Heavy Ion Collider (RHIC)

and CERN's Large Hadron Collider (LHC) are two such facilities where QGP can be created by colliding nuclei. The detection of QGP in heavy-ion collisions (HIC) at RHIC and LHC energies is one of the most challenging tasks for both experimentalists and theorists working in this field, primarily because of the extremely transient nature of the QGP.

Collisions between two nuclei at relativistic energies will create charged particles – either in the partonic or in the hadronic phase depending on the colliding energy. Interactions among these charged objects will produce real photon and lepton pairs. Photons and leptons interact electromagnetically. Therefore, their mean free paths are larger than the size of the system and hence can bring information on the state of the emission point very efficiently. Photon and lepton pairs emitted from the QGP are oblivious to the hadronic phase that appears during the evolution of the matter due to phase transition. As a consequence, their emissions from QGP *vis-à-vis* hot hadronic matter are considered as efficient diagnostic tools of q–h transition [2–4] (see also [5–7]) and this is the focus of the present article. The deviation between the photon spectra (or lepton pairs) originating from QGP and hadronic phases in the momentum space may be used as a probe for QGP. In relativistic heavy-ion collisions, most of the photon and dilepton spectra are measured in the central rapidity ($y = 0$) region, i.e., spectra are described by the transverse momentum ($p_{\rm T}$) of the photons.

The QGP evolves dynamically in space and time due to high internal pressure. Consequently, the system cools fast and reverts to hadronic matter. At the formation time, the entire energy of the system is thermal in nature and as time progresses, some part of the thermal energy gets converted to the collective (flow) energy. In other words, during the expansion, the total energy of the system is shared by the thermal as well as the collective degrees of freedom. The evolution of collectivity within the system is sensitive to the equation of state (EoS). Therefore, the study of the collectivity in the system will be useful to shed light on the EoS (see [8–11] for reviews) and on the nature of the transition taking place during the evolution process if the system is formed in QGP. It is well known that the average magnitude of radial flow at the freeze-out surface can be extracted from the $p_{\rm T}$ spectra of the hadrons. However, hadrons being strongly interacting objects can bring the information of the state of the system when it is too dilute to support collectivity, i.e., the parameters of collectivity extracted from the hadronic spectra are limited to the evolution stage where the collectivity ceases to exist. These collective parameters have hardly any direct information about the interior of the matter. Therefore, a suitable dynamical model is required for the final hadronic spectra to extrapolate backward in time to learn about the state of the initial hot/dense phase. In contrast to hadrons, the electromagnetic (EM) probes, i.e., photons and dileptons, are produced and emitted from each space-time point and therefore, EM probes will shed light on how both the radial [12] and elliptic flows [13–16] develop in the system. For dilepton, apart from $p_{\rm T}$ there is an additional kinematic variable, i.e., the invariant mass (M) – out of these two variables, $p_{\rm T}$ is not a Lorentz scalar and hence is changed by the expansion of the system but M being a Lorentz scalar is not affected by the flow. Moreover, the high M pairs are predominantly emitted from early times and the low M pairs from late time. Therefore, a judicious choice of $p_{\rm T}$ and M window will enable one to study the evolution of the flow in the medium. In this context, lepton pairs may also be used to understand the evolution of elliptic flow in the system.

This review is organized as follows. In the next section we discuss the emissions of photon and lepton pairs from the system formed in heavy-ion collisions. In §3, the space-time evolution of the matter produced in HIC is described. Section 4 is devoted to discuss results on photon, lepton pair spectra and elliptic flow of electromagnetic probes. In §5 suppression of heavy quarks in QGP measured through the p_{T} spectra of heavy flavoured mesons are mentioned briefly. Sections 6 deals with the summary and discussions.

2. Photon and dilepton production in heavy-ion collisions

In heavy-ion collisions (HIC), photons and dileptons are produced by various mechanisms at various stages of the evolution. These are broadly categorized as: (i) productions of photons and dileptons from the interactions of the partons of the colliding nuclei (while the photon spectra originated from these collisions are called prompt photons [17], the lepton pairs are known as Drell–Yan pairs [18]) (see [19] for a review), (ii) thermal productions – from the interactions of thermal partons as well as from thermal hadrons and (iii) finally from the decays of the long (compared to strong interaction time-scale) lived mesons. There are non-negligible contributions in the intermediate M distributions of lepton pairs from the decays of heavy flavoured mesons, charm and bottom.

2.1 *Prompt photons*

In the relativistic heavy-ion collision, the high p_{T} prompt photons originate from the following reactions of the partons of the colliding nuclei: (i) the Compton scattering: $q(\bar{q}) + g \rightarrow q(\bar{q}) + \gamma$; (ii) quark–antiquark annihilation: $q + \bar{q} \rightarrow g + \gamma$ and quark (antiquark) fragmentation: $q(\bar{q}) \rightarrow q(\bar{q}) + \gamma$. The invariant cross-section of the photons from a hadronic reaction ($a + b \rightarrow \gamma +$ anything) can be written in the factorized form as follows [20]:

$$E\frac{\mathrm{d}\sigma}{\mathrm{d}^3p} = \sum_{i,j,k}\int\Bigg[\mathrm{d}x_i\mathrm{d}x_j \; f_a^i(x_i,\mu)\,f_b^j(x_j,\mu)\times\Bigg\{E\frac{\mathrm{d}\hat{\sigma}(\mu,\mu_{\mathrm{R}},\mu_{\mathrm{F}})}{\mathrm{d}^3p}(i+j\rightarrow\gamma) + \int \mathrm{d}z_k E\frac{\mathrm{d}\hat{\sigma}}{\mathrm{d}^3p}(i+j\rightarrow k)D_\gamma^k(z_k,\mu_{\mathrm{F}})\Bigg\}\Bigg], \tag{1}$$

where f is the structure function, $\hat{\sigma}$ is the hard cross-section for the photon producing processes, D_γ^k is the fragmentation function of the parton, and k to γ, μ, μ_{F} and μ_{R} are the factorization, fragmentation and renormalization scales respectively. The first term in eq. (1) stands for the direct partonic process (i.e., Compton scattering and annihilation processes of quark and antiquark) and the second term represents quark (antiquark) fragmentation process.

The prompt photon $p_{\rm T}$ spectrum for the nucleus–nucleus (A–A) interaction is expressed in terms of p+p collisions as follows:

$$\frac{{\rm d}N^{AA}}{{\rm d}^2p_{\rm T}{\rm d}y} = T_{AA}(b)\frac{{\rm d}\sigma^{pp}}{{\rm d}^2p_{\rm T}{\rm d}y}, \tag{2}$$

where $T_{AA}(b) = N_{\rm coll}(b)/\sigma_{\rm in}^{pp}$, $T_{AA}(b)$ is the thickness function, $N_{\rm coll}(b)$ is the number of inelastic nucleon–nucleon collisions and $\sigma_{\rm in}^{pp}$ is the inelastic cross-section of pp interaction.

2.2 *Drell–Yan processes*

The process of high-mass ($M > 3$ GeV) lepton pairs emerging from $q\bar{q}$ annihilation in hadronic collisions ($a + b \rightarrow l^+ + l^- +$ anything) is described by Drell–Yan process and is the best understood part of dilepton production. In parton model, the invariant cross-section for large mass lepton pairs in hadronic collisions is given by

$$\frac{{\rm d}^2\sigma}{{\rm d}M^2{\rm d}y} = \frac{8\pi\alpha^2}{9Ms}\sum_{\rm q} e_{\rm q}^2\left[f_{\rm q}^a(x_1,\mu)f_{\bar{\rm q}}^b(x_2\mu) + f_{\bar{\rm q}}^a(x_1,\mu)f_{\rm q}^b(x_2,\mu)\right], \tag{3}$$

where M is the mass of the lepton pair and s is centre-of-mass energy of colliding hadrons. Equation (3) represents a purely electromagnetic process. The distribution of lepton pairs show no $p_{\rm T}$ dependence because QCD interaction between q and $\bar{q}$ is neglected here. The emission or absorption of a gluon by the initial-state partons will generate transverse momentum for the lepton pairs through conservation of linear momentum. Leading-order processes relevant for the $p_{\rm T}$ generation of the dileptons are: $q\bar{q} \rightarrow gl^+l^-$ (annihilation) and $q(\bar{q})g \rightarrow q(\bar{q})l^+l^-$ (Compton). The transverse momentum of the dileptons can also be generated by the intrinsic transverse motion of the partons inside the hadrons due to its finite size. However, the effects of the intrinsic transverse momentum is found to be negligible at very high-energy hadronic collisions (especially for the RHIC and the LHC energies).

The other important source of lepton pairs is the correlated decay of D and $\bar{D}$ [21]. At LHC this contribution is the most dominant one at intermediate M [22]. These contributions in HIC can also be estimated by scaling up the yield from pp collisions by $N_{\rm coll}$.

2.3 *Production of thermal photons and lepton pairs – general principle*

The number of thermal lepton pairs produced in the system (formed after a high-energy nuclear collision) per unit space-time volume per unit four-momentum volume is given by [2–4]

$$\frac{{\rm d}N}{{\rm d}^4p{\rm d}^4x} = \frac{\alpha}{12\pi^4M^2}L(M^2){\rm Im}\Pi_\mu^{{\rm R}\mu}f_{\rm BE}, \tag{4}$$

α is the EM coupling, ${\rm Im}\Pi_\mu^\mu$ is the imaginary part of the retarded photon self-energy and $f_{\rm BE}$ is the Bose–Einstein factor which is a function of $u^\mu p_\mu$ for a thermal system having four-velocity u^μ at each space-time point of the system, $p^2(= p_\mu p^\mu) = M^2$ is the invariant mass square of the lepton pair and

$$L(M^2) = \left(1 + \frac{2m^2}{M^2}\right)\sqrt{1 - 4\frac{m^2}{M^2}} \tag{5}$$

arises from the final-state leptonic current involving Dirac spinors and m in eq. (5) is the lepton mass.

The real photon production rate can be obtained from the lepton pair emission processes by replacing the product of the EM vertex $\gamma^* \rightarrow l^+l^-$, the term involving final-state leptonic current and the square of the (virtual) photon propagator by the polarization sum ($\sum_{\text{polarization}} \epsilon^\mu \epsilon^\nu = -g^{\mu\nu}$) for the real photon. Finally, the phase-space factor for the lepton pairs should be replaced by that of the photon to obtain the photon emission rate as

$$E\frac{\mathrm{d}N}{\mathrm{d}^4x\mathrm{d}^3p} = \frac{g^{\mu\nu}}{(2\pi)^3}\mathrm{Im}\Pi_{\mu\nu}f_{\mathrm{BE}}. \tag{6}$$

The results given above is correct up to order $e^2(\sim\alpha)$ in EM interaction but exact, in principle, to all order in strong interaction. Now it is clear from eqs (4) and (6) that for the evaluation of photon and dilepton production rates one needs to evaluate the imaginary part of the photon self-energy. The thermal cutting rules give a systematic procedure to express the imaginary part of the photon self-energy in terms of the physical amplitude.

2.3.1 *Thermal photons from quark gluon plasma.* The contribution from QGP to the spectrum of thermal photons due to annihilation ($q\bar{q} \rightarrow g\gamma$) and Compton ($q(\bar{q})g \rightarrow q(\bar{q})\gamma$) processes has been calculated in [23,24] using hard thermal loop (HTL) approximation [25]. Later, it was shown that photons from the processes [26]: $gq \rightarrow gq\gamma$, $qq \rightarrow qq\gamma$, $qq\bar{q} \rightarrow q\gamma$ and $gq\bar{q} \rightarrow g\gamma$ contribute in the same order $O(\alpha\alpha_{\mathrm{s}})$ as Compton and annihilation processes. The complete calculation of emission rate from QGP to order α_{s} has been performed by resuming ladder diagrams in the effective theory [27]. This rate has been used for obtaining the results to be displayed here. The T dependence of the strong coupling α_{s} has been taken from [28].

2.3.2 *Thermal photons from hadrons.* For the photon spectra from hadronic phase, an exhaustive set of hadronic reactions and the radiative decay of higher resonance states are considered [29–31]. The relevant reactions and decays for photon production are: (i) $\pi\,\pi \rightarrow \rho\,\gamma$, (ii) $\pi\,\rho \rightarrow \pi\gamma$ (with all possible mesons in the intermediate state [31]), (iii) $\pi\,\pi \rightarrow \eta\,\gamma$ and (iv) $\pi\,\eta \rightarrow \pi\,\gamma$, $\rho \rightarrow \pi\,\pi\,\gamma$ and $\omega \rightarrow \pi\gamma$. The corresponding vertices are obtained from various phenomenological Lagrangians described in detail in refs [29–31]. The reactions involving strange mesons, $\pi\,K^* \rightarrow K\,\gamma$, $\pi\,K \rightarrow K^*\gamma$, $\rho\,K \rightarrow K\,\gamma$ and $K\,K^* \rightarrow \pi\,\gamma$ [33] have also been incorporated in the present work. Contributions from other decays, such as $K^*(892) \rightarrow K\,\gamma$, $\phi \rightarrow \eta\,\gamma$, $b_1(1235) \rightarrow \pi\,\gamma$, $a_2(1320) \rightarrow \pi\,\gamma$ and $K_1(1270) \rightarrow \pi\,\gamma$ have been found to be small [32] for $p_{\mathrm{T}} > 1$ GeV. All the isospin combinations for the above reactions and decays have properly been taken into account. The effects of hadronic form factors [33] have also been incorporated in the present calculation.

2.4 *Thermal dileptons*

As mentioned before, lepton pairs can be used as efficient probes for QGP diagnostics, provided one can subtract out contributions from Drell–Yan process, decays of vector mesons within the lifetime of the fire ball and hadronic decays occurring after the

freeze-out. Like hard photons, lepton pairs from Drell–Yan processes can be estimated by pQCD. The $p_{\rm T}$ spectra of thermal lepton pairs suffer from the problem of indistinguishability between QGP and hadronic sources unlike the usual invariant mass (M) spectra which show characteristic resonance peaks in the low M region. The invariant transverse momentum distribution of thermal dileptons (l^+l^- or virtual photons, γ^*) is given by

$$\frac{{\rm d}^2N}{{\rm d}^4x\,{\rm d}^2p_{\rm T}{\rm d}y} = \sum_{i=Q,M,H}\int_i\left(\frac{{\rm d}^2N_{\gamma^*}}{{\rm d}^2p_{\rm T}{\rm d}y{\rm d}M^2{\rm d}^4x}\right)_i {\rm d}M^2. \tag{7}$$

The lower (M_1) and upper (M_2) limits of M integration can be fixed judiciously to detect contributions from either quark matter or hadronic matter. Experimental measurements [34,35] are available for different M windows.

2.5 *Dilepton emission from QGP*

In the QGP phase, the lowest order process producing lepton pair is $q\bar{q} \to \gamma^* \to l^+l^-$ [36]. QCD corrections to this lowest order rate is obtained in [37] (see also [38]) in the weak coupling limit, i.e. for very low values of strong coupling, $\alpha_{\rm s}$. The value of $\alpha_{\rm s}$ becomes small in the QCD plasma at very high temperatures. Such a high-temperature limit cannot be achieved by colliding nuclei at RHIC and LHC energies. Therefore, these results may not be very useful to analyse the currently available experimental data. It is important to mention here that this is also true for the photon emission rate (although we have used it here in the absence of any better results) which is derived in the weak coupling limit within the framework of hard thermal loop approximations discussed earlier. The emission rate from QGP in the strong coupling limit may be achieved by lattice QCD calculations. Indeed, the dilepton emission rate has been obtained from lattice QCD calculations for $T > T_{\rm c}$ [39] (see also [40]). The future lattice QCD results with dynamical quarks will be very useful to analyse experimental data from HIC at relativistic energies.

2.6 *Dilepton emission from the hadronic medium*

The thermal lepton pairs in HIC originate from the decays of low-mass vector mesons (ρ, ω and ϕ). Using the relation between hadronic electromagnetic current and the vector meson field through field current identity, one can express the emission rate of low-mass lepton pairs in terms of in-medium spectral functions of light vector mesons as follows (see [41] for details):

$$\frac{{\rm d}N}{{\rm d}^4p{\rm d}^4x} = -\frac{\alpha^2}{\pi^3p^2}f_{\rm BE}(p_0)\sum_{V=\rho,\omega,\phi}F_V^2m_V^2A_V(p_0,\vec{p}), \tag{8}$$

where F_V is the coupling between the electromagnetic current and the vector meson (V), m_V is the mass and A_V is the spectral function of V respectively in the hadronic medium at non-zero temperature and density. The change of spectral function of ρ due to its interaction with π, ω, a_1, h_1 (see [41,42] for details) and baryons [43] have been included to evaluate the production of lepton pairs from HM. For the ω spectral function, the width at non-zero temperature is taken from ref. [44] and medium effects on ϕ is ignored. In

addition, the ρ and ω spectral functions are augmented by contributions from continuum [7,45] and hence the reactions like four-pion annihilation [46] are ignored to avoid double counting. The continuum is parametrized as indicated in [7].

2.7 *Thermal photons and dileptons from an expanding medium*

Ideally, one wants to detect photons from QGP. However, the experimental data contain photons from various processes, e.g. from the hard collisions of initial-state partons of the colliding nuclei, thermal photons from quark matter and hadronic matter and photons from the hadronic decays after freeze-out. The contributions from the initial hard collisions of partons can be estimated by using eq. (2). Photons from the hadronic decays ($\pi^0 \rightarrow \gamma\gamma$, $\eta \rightarrow \gamma\gamma$ etc.) can be reconstructed, in principle, by invariant mass analysis. But the most challenging task is to separate the thermal photons originating from the expanding hadrons.

Similarly, the dilepton yield from the expanding system under consideration is obtained by convoluting the static rate by integrating over the four-volume, d^4x for a system undergoing radial and longitudinal expansions with cylindrical symmetry [48] and boost invariance along longitudinal direction [47].

The invariant momentum distribution of thermal photons or dileptons (generically denoted by $\mathrm{d}^2N/\mathrm{d}^2p_\mathrm{T}\mathrm{d}y$) can be written as

$$\frac{\mathrm{d}^2N}{\mathrm{d}^2p_\mathrm{T}\mathrm{d}y} = \sum_{i=Q,M,H} \int_i \left(\frac{\mathrm{d}^2N}{\mathrm{d}^2p_\mathrm{T}\mathrm{d}y\mathrm{d}^4x}\right)_i \mathrm{d}^4x, \tag{9}$$

where $i \equiv Q, M, H$ represents QGP, mixed (coexisting phase of QGP and hadrons) and hadronic phases respectively. $(\mathrm{d}^2N/\mathrm{d}^4x\mathrm{d}^2p_\mathrm{T}\mathrm{d}y)_i$ is the static rate of photon production from the phase i, which is convoluted over the expansion dynamics by integrating over d^4x. Dilepton yield from an expanding system can similarly be obtained.

3. Space-time dynamics of HIC

The space-time evolution of the system formed in HICs can be studied by using relativistic hydrodynamics, by assuming that the system reaches the state of equilibrium at a time τ_i after the collision. The evolution of the fluid is governed by the energy–momentum conservation equation:

$$\partial_\mu T^{\mu\nu} = 0, \tag{10}$$

where $T^{\mu\nu} = (\epsilon + P)u^\mu u^\nu + g^{\mu\nu}P$ is the energy–momentum tensor for the ideal fluid, ϵ is the energy density, P is the pressure and u^μ is the fluid four-velocity. Using eq. (10) and the second law of thermodynamics, one can show that for an isentropic non-viscous flow, the entropy conservation law reads as

$$\partial_\mu s^\mu = 0, \tag{11}$$

where $s^\mu = s\,u^\mu$ is the entropy current. For fluid containing non-zero baryon number, one needs to solve the equation:

$$\partial_\mu (n_\mathrm{B}u^\mu) = 0 \tag{12}$$

simultaneously with eq. (10). In eq. (12), n_B is the baryon density. However, for HIC at RHIC and LHC energies, the net baryon at the central rapidity region is found to be small and hence eq. (12) can be ignored and in such a scenario only eq. (10) is required to be solved. To solve eq. (10) for HIC, the initial condition and equation-of-state (EoS) are to be prescribed and also the conditions as to where the evolution needs to be stopped have to be specified (freeze-out condition). The hydrodynamical equation, eq. (10) is solved with boost invariance [47], along longitudinal direction and azimuthal symmetry [48] to estimate the p_T and M distributions of electromagnetic probes. However, while evaluating the elliptic flow, v_2 of the lepton pairs, the assumption of azimuthal symmetry is relaxed [49].

The initial temperature T_i can be related to the measured hadronic multiplicity (dN/dy) by the following relation for a system undergoing isentropic expansion [50]:

$$\frac{dN}{dy} = \pi R_A^2 4 a_q T_i^3 \tau_i / c, \tag{13}$$

where R_A is the radius of the colliding nuclei, c is a constant ($\sim$4) and $a_q = (\pi^2/90)\times$ statistical degeneracy. For example, in QGP phase, the statistical degeneracy, $g_q = 2 \times 8 + 7 \times 2 \times 2 \times 3 \times N_F/8$, N_F is the number of flavours. The value of dN/dy can be estimated from the following equation [51]:

$$\frac{dN}{dy} = (1-x)\frac{dn_{pp}}{dy}\frac{\langle N_{part}\rangle}{2} + x\frac{dn_{pp}}{dy}\langle N_{coll}\rangle. \tag{14}$$

N_{coll} is the number of collisions which contribute x fraction to the multiplicity dn_{pp}/dy measured in pp collision. The number of participants N_{part} contributes a fraction $(1-x)$ of dn_{pp}/dy. The values of N_{part} and N_{coll} are estimated by using Glauber model. The hydrodynamical equations describing the radial as well as the longitudinal expansions of the system are solved with the following initial conditions. The radial dependence of the initial energy density profile is taken as

$$\epsilon(\tau_i, r) = \frac{\epsilon_0}{1 + \exp(\frac{r - R_A}{\delta})}, \tag{15}$$

where δ is the surface thickness taken as 0.5 fm in the present calculation. The initial radial velocity profile is assumed to be: $v_r(\tau_i, r) = 0$. The energy density in the plateau region ϵ_0 is estimated from the value of the initial temperature T_i by using the relation $\epsilon = g_q \pi^2/30 \times T_i^4$.

The lattice QCD EoS [52] for the QGP phase and hadronic resonance gas EoS for the hadronic phase [53] have been used. The kinetic freeze-out temperature can be constrained by the p_T spectra of hadrons. The ratios of various hadrons measured experimentally at different $\sqrt{s_{NN}}$ indicate that the system produced in HIC decouple chemically at $T_{ch}(>T_f)$. Therefore, the system remains out of chemical equilibrium from T_{ch} to T_f. The deviation of the system from the chemical equilibrium is taken into account by introducing chemical potential for the relevant hadronic species [54].

4. Results

Having specified various processes for photon and dilepton productions from QGP and hot hadrons, we are ready to evaluate their spectra originating from the expanding system

with the help of relativistic hydrodynamics solved using the initial conditions and EoS mentioned earlier.

4.1 *Transverse momentum spectra of photons*

The efficiency of photons for being considered as a competent probe of QGP largely depends on the ability to disentangle the photons produced from various stages of evolution of the system formed in HIC. Therefore, first we identify the possible sources of photons above those coming from the decays of π^0, η mesons etc. as provided by the data. As photons from these decays are already eliminated from the experimental data from SPS, RHIC and LHC experiments, these need not be considered. Therefore, the following sources of photons are going to be considered here:

(i) Prompt photons: produced from the initial hard collisions of the partons from the nucleons of the colliding nuclei. This contribution may be estimated by using the techniques of perturbative QCD (pQCD) and the data from *pp* collisions may be used to validate such calculations. The p_{T} distributions of photons from proton+proton (*pp*) collisions at a given energy can be used as a benchmark for the hard contribution in HIC. Therefore, estimation of these contributions with minimal model dependence is important. In view of this, in the present analysis, we estimate the high p_{T} contributions in HIC by using the procedure outlined in [59], i.e., use the data from *pp* collisions and scale it up by the number of collisions in nucleus–nucleus interactions.

(ii) Photons are also produced from the interactions of the pre-equilibrated partons, i.e., from the time span between the collision point and the onset of thermalization. If the thermalization time-scale is very small (as in the case of RHIC and LHC), the contributions from this interval will be insignificant and hence can be neglected. Michler *et al* [55] have done an interesting work recently to understand the photon production during the chiral phase transition of the system formed just after HIC.

(iii) Thermal photons originating from the interactions of (a) quarks and gluons and (b) thermal hadrons (π, ρ, η, ω, a_1 etc.) in the bath. The estimation of the thermal contribution depends on the space-time evolution scenario. In the case of a deconfinement phase transition, which seems to be plausible at the RHIC and the LHC energies, one assumes that QGP is formed initially. The equilibrated plasma then expands, cools and reverts to hadronic matter and finally freezes out. Evidently, there will be thermal radiation from QGP as well as from the luminous hadronic fireball which has to be estimated as accurately as possible to have a reliable estimate of the initial temperature.

The momentum distributions of photons (and dileptons) produced from a thermal system depend on the temperature T of the source through the thermal phase-space factors of the participants of the reactions [56]. Consequently, the transverse momentum p_{T} spectra of photon reflects the temperature of the source. For an expanding system the situation is, however, more complex. With the onset of transverse flow, the quarks and gluons in the system will yield momenta in the transverse direction in addition to their momenta due to

thermal motion. Consequently, the conservation of momentum will ensure a transverse momentum gain by the photons produced from the interactions of quarks and gluons in the expanding medium. Therefore, the transverse flow (characterized by radial flow velocity, v_r) will modify the p_T distribution of the photons. This will make the photons originating from the hadronic phase with low T ($< T_c$) but high v_r to possibly mix with photons produced from the QGP with relatively high T but low v_r [57]. Consequently, the intermediate or the high p_T part of the spectra will contain contributions from both QGP as well as hadrons making the disentanglement of photons from QGP very difficult. The photon spectra measured experimentally represent the space-time integrated yield from the matter that evolves from an initial hot and dense phase to a comparatively cooler and diluted phase of hadronic gas. Therefore, the temperature extracted from such spectra will exhibit the average temperature of the system.

The direct photon spectra from Pb+Pb collisions is measured at $\sqrt{s_{NN}} = 2.76$ TeV by ALICE Collaboration [58]. However, no data at this collision energy are available for pp interactions. Therefore, prompt photons from $p + p$ collision at $\sqrt{s_{NN}} = 7$ TeV has been used to estimate the hard contributions for nuclear collisions at $\sqrt{s_{NN}} = 2.76$ TeV by using the scaling procedure (with $\sqrt{s_{NN}}$) used in [59]. For the Pb+Pb collisions, the result has been scaled up by the number of collisions at this energy (this is shown in figure 1 as prompt photons). The high p_T part of the data is reproduced by the prompt contributions reasonably well. At low p_T, the hard contributions underestimate the data indicating the presence of a possible thermal source.

The thermal photons with an initial temperature of ∼553 MeV ($\tau_i = 0.1$ fm/c) along with the prompt contributions explain the data well (figure 1), with the inclusion of non-zero chemical potentials for all hadronic species considered [54]. The average temperature extracted from the inverse slope of the spectra is ∼300 MeV as compared to the values 245 [60,61] and 265 [60,62] from the analysis of data obtained from SPS [59] and RHIC [63] collision conditions respectively.

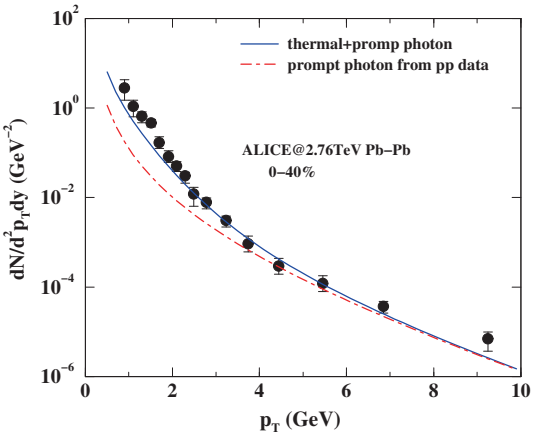

Figure 1. Transverse momentum spectra of direct photon at 2.76 TeV energy for Pb+Pb collision at 0–40% centrality (see [60] for details).

4.2 *Invariant mass and transverse momentum distribution of lepton pairs*

The p_T-integrated invariant mass spectra of dilepton is displayed for LHC initial conditions in figure 2. Dileptons from hot hadronic matter outshines the QGP for $M < m_\phi$ when the thermal effects on the ρ spectral function are included. For large M, however, the dileptons from QGP dominates. To show the sensitivity of the results on the EoS, we display the results for HRG (hadronic resonance gas) EoS and contrast it with results obtained from lattice QCD EoS. HRG EoS is obtained by including all the hadrons upto 2.5 GeV mass in the energy density and pressure of the hadronic system and bag model EoS for the QGP. For RHIC, the results (see ref. [64]) are qualitatively similar to LHC. However, quantitatively the yield at RHIC is lower [42] because of the larger four-volume of the system to be realized at LHC resulting from a higher value of T_i for fixed T_c and T_F. A large enhancement in the dilepton yield is observed as a result of broadening of the ρ spectral function due to the inclusion of $\pi\pi$, $\pi\omega$, πa_1 and πh_1 loops and the ρ-nucleon interactions. In figure 3, the transverse momentum distribution of lepton pairs for various average M ($M_{av} = (M_1 + M_2)/2$, where M_1 and M_2 are the upper and lower limits of M). In confirmation with the results displayed in figure 2, we observe that the spectra for $M_{av} \sim 0.3$ and ρ-peak are similar and dominate over the spectra for other M_{av} values for the entire p_T range. Therefore, an appropriate selection of M and p_T will be very useful to extract various properties (effective temperature, average flow, etc.) of the QGP or the hadronic phase.

Finally, the variation of inverse slope of the M_T distributions with M_{av} for LHC is depicted in figure 4. The values of T_{eff} for various M-bins are larger than RHIC because of the combined effects of large initial temperature and flow. In fact, the value of the radial velocity v_r for $0.5 < M(\text{GeV}) < 0.77$ is $\sim$0.52 compared to 0.25 at RHIC [42]. The radial flow in the system is responsible for the rise and fall of T_{eff} with M_{av} (solid line) in the mass region $0.5 < M(\text{GeV}) < 1.3$, for $v_r = 0$ (dashed line) a completely different behaviour is obtained. This type of non-monotonic variation of T_{eff} cannot be obtained with a single dilepton source [65]. Therefore, such non-monotonic variation of the inverse slope deduced from the transverse mass distribution of lepton pairs with

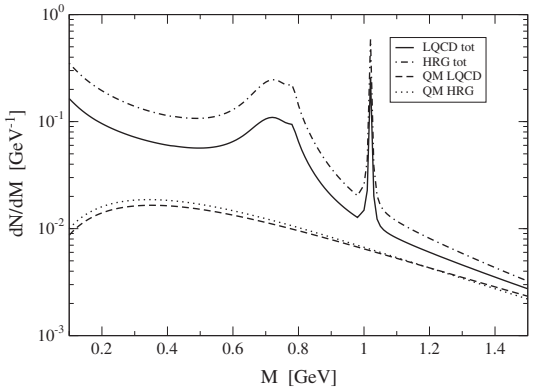

Figure 2. Dilepton yields for HRG EoS and LQCD EoS. The initial condition is taken for LHC energy (taken from [41]).

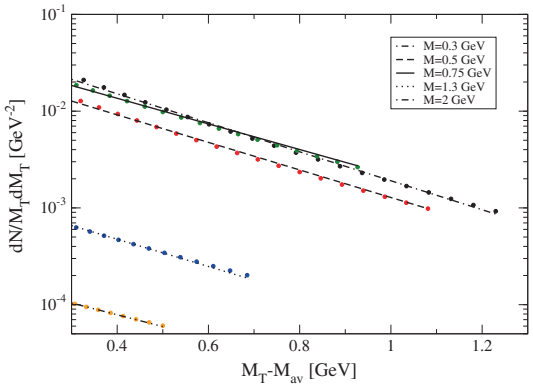

Figure 3. The dilepton yield plotted against $M_{\rm T} - M_{\rm av}$ for different M windows for LHC initial condition (taken from [42]).

average invariant mass is an indication of the presence of two different phases during the evolution of the system. Thus, such variation may be treated as a signal of QGP formation in heavy-ion collisions. Photon spectra may be used to make a connection between $T_{\rm eff}$ and true temperature of the evolving matter [66].

The other sources of dileptons e.g., the Drell–Yan (DY) mechanism and charm decays, may provide significant 'background' to the thermal productions at high mass region ($2 \leq M$ (GeV) ≤ 6 [67]) which are neglected here because in the present work we focus mainly on the low-mass regions. Moreover, the contributions from the DY process and charm decays from proton+proton (pp) collisions may be used to estimate similar contributions from heavy-ion collisions at the same colliding energy by appropriately scaling pp data by the effective number of nucleon+nucleon collisions in nuclear interaction. The contributions from the ρ at the freeze-out surface has been evaluated and it is found to be small [41].

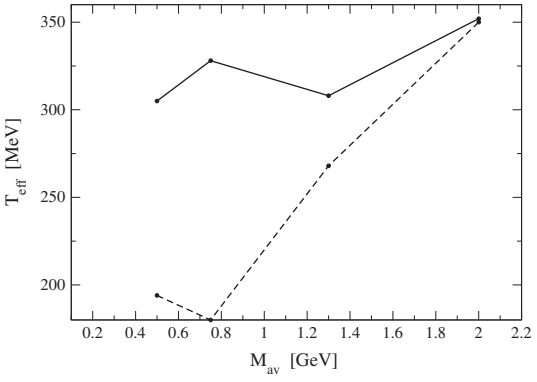

Figure 4. $T_{\rm eff}$ for different values of the M-bins for LHC conditions. The dashed line is obtained by setting $v_{\rm r} = 0$ (from [42]).

4.3 *Elliptic flow lepton pairs and photons*

Non-central heavy-ion collisions provide an anisotropic spatial configuration. Interactions among the constituents of the system develop pressure gradients of different magnitude along different spatial directions resulting in anisotropic flow velocity. With the expansion, the spatial anisotropy reduces and the momentum space anisotropy builds up rapidly. The v_2 is a measure of this momentum space anisotropy which is defined as: $v_2 = \langle p_x^2 - p_y^2\rangle/\langle p_x^2 + p_y^2\rangle$, where p_x and p_y are the x and y components of the particle momenta. In contrast to hadrons, which are predominantly emitted from the freeze-out surface of the fireball, the electromagnetically interacting particles are penetrating probes as mentioned earlier. Therefore, the analysis of v_2 of the lepton pairs [13,14,16] and photons [15] can provide information of the pristine stage of the matter produced in HIC. Similar to photons, as explained earlier in §4.1, the radial flow alters the shape of the $p_{\rm T}$ spectra of dileptons too. The presence of large radial flow may diminish the magnitude of v_2 at low $p_{\rm T}$ [68] and this effect will be larger when the radial flow is large, i.e. in the hadronic phase which corresponds to lepton pairs with $M \sim m_\rho$.

The v_2 of dileptons can also be used to test the validity and efficiency of the extrapolation required for hadronic v_2. The $p_{\rm T}$-integrated M distribution of lepton pairs with $M(>m_\phi)$ originating from the early time, providing information of the partonic phase and pairs with $M \lesssim m_\rho$ are chiefly produced later from the hadronic phase. Therefore, the $p_{\rm T}$-integrated M distribution of lepton pairs may be used as a chronometer of the heavy-ion collisions. On the other hand, the variation of v_2 with $p_{\rm T}$ for different M windows may be used as a flow-meter.

The elliptic flow of the dilepton, $v_2(p_{\rm T}, M)$ can be defined as

$$v_2 = \frac{\sum \int \cos(2\phi) \left(\frac{{\rm d}N}{{\rm d}^2 p_{\rm T} {\rm d}M^2 {\rm d}y}|_{y=0}\right) {\rm d}\phi}{\sum \int \left(\frac{{\rm d}N}{{\rm d}^2 p_{\rm T} {\rm d}M^2 {\rm d}y}|_{y=0}\right) {\rm d}\phi}, \tag{16}$$

where $\sum$ stands for summation over quark matter (QM) and hadronic matter (HM) phases. In this work dileptons from non-thermal sources e.g., from the Drell–Yan process and decays of heavy flavours [69] are ignored for evaluating the elliptic flow of lepton pairs from QM and HM. If the charm and bottom quarks do not thermalize, then they are not part of the flowing QGP and hence do not contribute to the elliptic flow. The model employed in the present work leads to a good agreement with NA60 dilepton data [34] for SPS collision conditions [70] (see [71] for a comprehensive discussion).

To evaluate v_2 from eq. (16), one needs to integrate the production rate over the space-time evolution of the system – from the initial QGP phase to the final hadronic freeze-out state through a phase transition in the intermediate stage. We assume that the matter is formed in QGP phase with negligible net baryon density. The initial condition required to solve the hydrodynamic equations for the description of the matter produced in Pb+Pb collision at $\sqrt{s_{NN}} = 2.76$ TeV for 30–40% centrality is as follows: $T_{\rm i} = 456$ MeV is the initial temperature corresponding to the maximum of the initial energy density profile at the thermalization time $\tau_{\rm i} = 0.6$ fm/c. The EoS required to close the hydrodynamic equations is constructed by complementing Wuppertal–Budapest lattice simulation [72] with a hadron resonance gas comprising all the hadronic resonances up to a mass of 2.5 GeV [53,73]. The energy of the lepton pair in the co-moving frame is given by:

$p \cdot u = \gamma_T(M_T \cosh(y - \eta) - v_x p_T \cos\phi - v_y p_T \sin\phi)$, where $u = (\gamma, \gamma\vec{v})$, is the fluid four-velocity, y is the rapidity and η is the space-time rapidity, $\gamma_T = (1 - v_r^2)^{-1/2}$, $v_r^2 = v_x^2 + v_y^2$, v_x and v_y are the x and y components of the velocity. The EoS and the values of the parameters mentioned above are constrained by the p_T spectra (for 0–5% centrality) and elliptic flow (for 10–50% centrality) of charged hadrons [73] measured by ALICE Collaboration [74].

Figure 5a and 5b show the differential elliptic flow $v_2(p_T)$ of dileptons arising from various $\langle M \rangle$ domains. We observe that for $\langle M \rangle = 2.5$ GeV, v_2 is small for the entire p_T range because these pairs arise dominantly from the QM epoch (see figure 2) when the flow is not developed fully. By the time (6–12 fm/c) the pairs are emitted predominantly from the region $\langle M \rangle = 0.77$ GeV, the flow which gives rise to large v_2 is fully developed. It is also interesting to note that the medium-induced enhancement of ρ spectral function provides a visible modification in v_2 for dileptons below ρ peak (figure 5c). The medium-induced effects lead to an enhancement of v_2 of lepton pairs which is culminating from the 'extra' interaction (absent when a vacuum ρ is considered) of the ρ with other thermal hadrons in the bath. We note that the differential elliptic flow $v_2(p_T)$ obtained here at LHC is larger than the values obtained at RHIC [15,16] for all the invariant mass windows. In figure 5d, we depict the variation of R_Q with p_T for $\langle M \rangle = 0.3$ GeV (line with solid circle), 0.77 GeV (solid line) and 2.5 GeV (line with open circle). The quantity R_Q (R_H) is defined as, $R_Q = v_2^{QM}/(v_2^{QM} + v_2^{HM})$ [$R_H = v_2^{HM}/(v_2^{QM} + v_2^{HM})$] where v_2^{QM} and v_2^{HM} are the elliptic flow of QM and HM respectively. The results clearly illustrate that v_2 of lepton pairs in the large $\langle M \rangle$(=2.5 GeV) domain (open circle in figure 5d) originate from QM for the entire p_T range considered here. The value of R_Q is large in this domain because

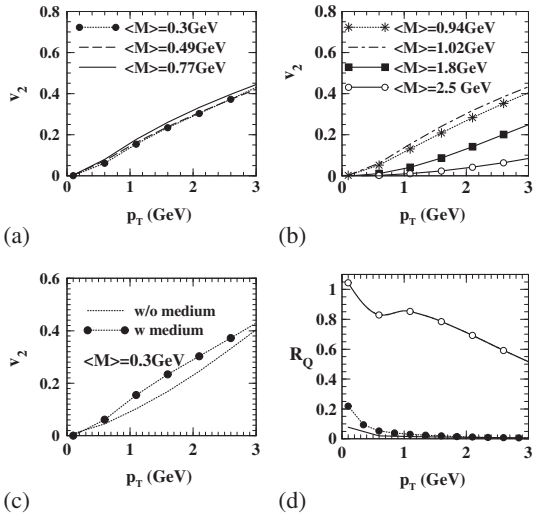

Figure 5. (**a**) and (**b**) indicate elliptic flow of lepton pairs as a function of p_T for various M windows. (**c**) displays the effect of the broadening of ρ spectral function on the elliptic flow for $\langle M \rangle = 300$ MeV. (**d**) shows the variation of R_Q (see text) with p_T for $\langle M \rangle = 0.3$ GeV (solid circle), 0.77 GeV (line) and 2.5 GeV (open circle). All the results displayed here are for 30–40% centrality (from [13]).

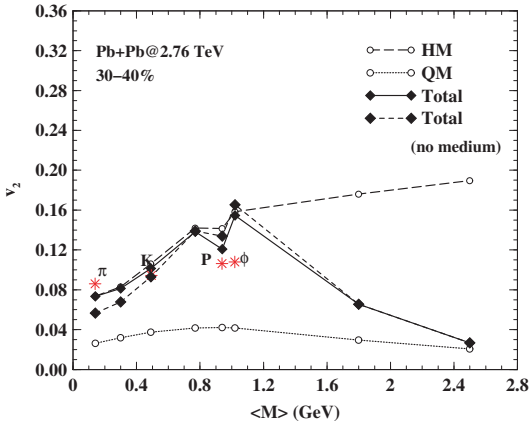

Figure 6. Variation of dilepton elliptic flow as function of $\langle M \rangle$ for QM, HM (with and without medium effects) and for the entire evolution. The symbol $*$ indicates the value of v_2 for hadrons e.g., π, kaon, proton and ϕ (from [13]).

of the large (negligibly small) contributions from QM (HM) phase. It is also clear that the contribution from QM phase to the elliptic flow for $\langle M \rangle$(=0.77 GeV) is very small (solid line in figure 3d). The value of R_H for $\langle M \rangle = 0.77$ GeV is large (not shown in the figure).

The v_2 at the HM phase (either at ρ or ϕ peak) is larger than its value in the QGP phase (at $\langle M \rangle = 2.5$ GeV, say) for the entire p_{T} range considered here. Therefore, the p_{T}-integrated values of v_2 should also retain this character at the corresponding values of $\langle M \rangle$, which is clearly observed in figure 6 which displays the variation of $v_2(\langle M \rangle)$ with $\langle M \rangle$. The v_2 of QM is small because of the small pressure gradient in the QGP phase. The v_2 resulting from hadronic phase has a peak around ρ pole indicating a large development of flow in the HM phase. For $\langle M \rangle > m_\phi$, the v_2 obtained from the combined phases approaches the value corresponding to v_2 for QGP. Therefore, measurement of v_2 for large $\langle M \rangle$ will bring information of the QGP phase at the earliest time of the evolution. It is important to note that the p_{T}-integrated $v_2(\langle M \rangle)$ of the lepton pairs with $\langle M \rangle \sim m_\pi, m_K$ is close to the hadronic v_2^π and v_2^K (symbol $*$ in figure 6). We also observe that the variation of $v_2(\langle M \rangle)$ with $\langle M \rangle$ has a structure similar to $\mathrm{d}N/\mathrm{d}M$ vs. M. This is because v_2 can be written as: $v_2(\langle M \rangle) \sim \sum_{\mathrm{i=QM,HM}} v_2^{\mathrm{i}} \times f_{\mathrm{i}}$, where f_{i} is the fraction of QM or HM from various space-time regions. The structure of $\mathrm{d}N/\mathrm{d}M$ is reflected in $v_2(\langle M \rangle)$ through f_{i}. We find that the magnitude of $v_2(\langle M \rangle)$ at LHC is larger than its value at RHIC.

5. Single electron from the heavy flavoured meson (HFM) decay

The heavy quarks (HQs) i.e., charm and bottom play vital roles in probing QGP. The HQs are produced in early time of the collision as their productions are associated with large momentum transfer. As the HQs are not frequently created or annihilated in the QGP, they can witness the entire space-time evolution of heavy-ion collision and act as

useful probes in QGP detection. HQs are not part of the bulk of the system as they are Boltzmann-suppressed due to their higher masses at the temperature range of a few hundred of MeV. This indicates that the interaction of HQs with QGP involves interactions between equilibrium (QGP) and non-equilibrium degrees of freedom (DoF). The Fokker–Planck (FP) equation provides an appropriate framework for such studies.

The interactions of HQs with QGP is encrypted in the depletion of high $p_{\rm T}$ hadrons (D and B) produced in nucleus + nucleus collisions relative to those produced in proton + proton ($p + p$) collisions. This depletion factor for a particle a, R_{AA} is defined as: $R_{AA}(p_{\rm T}) = {\rm d}N^{a\,{\rm Au+Au}}/{\rm d}^2p_{\rm T}{\rm d}y/\left[N_{\rm coll} \times {\rm d}N^{a\,pp}/{\rm d}^2p_{\rm T}{\rm d}y\right]$, R_{AA} can provide information on the properties of QGP. The STAR [75], PHENIX [76] and the ALICE [77] Collaborations have measured this high $p_{\rm T}$ depletion. In HIC the HQs suppression at high $p_{\rm T}$ are measured from the $p_{\rm T}$ distributions of electrons originating from their semileptonic decays of HFM at RHIC. Several ingredients like inclusions of non-perturbative effects from the quasihadronic bound state [78], 3-body scattering [79], the dissociation of heavy mesons due to its interaction with the thermal partons [80] and employment of running coupling constants and realistic Debye mass [81] have been proposed to improve the description of the experimental data. Wicks *et al* [82] showed that the inclusion of both elastic and inelastic collisions and the path length fluctuation reduces the gap between the theoretical and experimental results.

The FP equation describing the motion of the HQs in the QGP reads as [83,84] (for an alternative scenario, see [85]),

$$\frac{\partial f}{\partial t} = \frac{\partial}{\partial p_i}\left[A_i(p)f + \frac{\partial}{\partial p_j}[B_{ij}(p)f]\right], \tag{17}$$

where f is the momentum distribution of the HQs describing the non-equilibrium DoF. A_i and B_{ij} are drag and momentum diffusion coefficients. The interaction between the probe and the medium enter through the drag and diffusion coefficients.

The momentum diffusion coefficient is a measure of the ability of mixing high-momentum zone with low-momentum zone, similar to the mass diffusion from high-density region to the low-density region. The transfer of momentum depends on the strength of the interaction and this can be used to assess the nature of the fluid – liquid or gas. Moreover, the shear viscosity of the system also signifies the ability to transfer momentum over a length scale $\sim$ mean free path, indicating that the coefficients of diffusion and shear viscosity are related quantities [86] (see ref. [87] for a review and references therein). During their propagation through the QGP, the HQs dissipate energy predominantly by two processes [88,89]: (i) collisional, e.g. $gQ \to gQ$, $qQ \to qQ$ and $\bar{q}Q \to \bar{q}Q$, and (ii) radiative processes, i.e., $Q+q \to Q+q+g$ and $Q+g \to Q+g+g$. The radiative loss is subjected to the dead cone and Landau–Pomeronchuk–Migdal (LPM) effects. Both radiative and collisional processes of energy loss are included in the effective drag and diffusion coefficients here. The initial HQ distribution has been taken from the NLO perturbative calculations [90]. In the present formalism, the suppression of high $p_{\rm T}$ D or B mesons in the QGP phase is given by

$$R_{AA} = \frac{f_Q}{f_{\rm i}}, \tag{18}$$

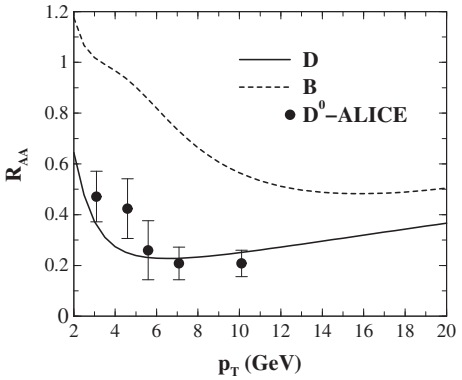

Figure 7. R_{AA} as a function of p_{T} for D and B mesons at LHC (experimental data are taken from [77] and theoretical results are taken from the second reference of ref. [88]).

where f_Q is given by the convolution of the solution of the FP equation at the end of the QGP phase (at $T_{\mathrm{c}} \sim 170$ MeV) with the HQ fragmentation to D or B mesons [91]. Similarly, f_{i} is the function obtained from the convolution of the initial heavy quark momentum distribution with the HQ fragmentation function for heavy mesons.

The p_{T} distribution will be unity in the absence of rescattering. Theoretical results have been compared with the recent ALICE data (ref. [77]) in figure 7. The data are reproduced well by assuming the formation of QGP at an initial temperature of ∼550 MeV and $\tau_{\mathrm{i}} = 0.1$ fm/c after Pb+Pb collisions at $\sqrt{s_{NN}} = 2.76$ TeV. The spectra evaluated using the formalism described above reproduce the data reasonably well (figure 7), with initial temperature $T_{\mathrm{i}} = 550$ MeV and thermalization time $\tau_{\mathrm{i}} = 0.1$ fm/c. The STAR [75] and the PHENIX [76] Collaborations have measured the $R_{AA}(p_{\mathrm{T}})$ for non-photonic single electron as a function of p_{T} for Au+Au at $\sqrt{s_{NN}} = 200$ GeV. The experimental data from both the collaborations show $R_{AA} < 1$ for $p_{\mathrm{T}} \geq 2$ GeV, indicating substantial interaction of the heavy quarks with the plasma particles.

6. Summary and outlook

In this review, the suitability of photons and lepton pairs as diagnostic tools for quark gluon plasma has been discussed. Theoretical results for LHC have been displayed and compared with the available experimental data. For RHIC and SPS, appropriate references have been provided. Experimental data from SPS and RHIC on both photons and lepton pairs have helped enormously to fine-tune parameters of various phenomenological models. It has also been possible to reject some of the theoretical models with the help of these data. For example, the NA60 data on invariant mass distributions of muon pairs rule out the reduction of ρ mass in the medium according to the scaling law proposed by Brown and Rho [93]. With an order of magnitude increase in collision energy at LHC, a much deeper understanding of the properties of primordial matter that existed in the early Universe is expected. Experimental data from LHC will enhance our understanding of photon productions from jet–plasma interaction [92] and glasma state [94]. Data

from CBM experiment [95] will help in understanding photons from baryon-rich plasma [96]. However, much more work is required to be done theoretically to understand the production of photons and leptons from non-equilibrated QCD plasma.

Acknowledgements

This work is a result of collaboration with Trambak Bhattacharyya, Asis Kumar Chaudhuri, Santosh Kumar Das, Sabyasachi Ghosh, Surasree Mazumder, Sukanya Mitra, Bedangadas Mohanty, Payal Mohanty and Sourav Sarkar. The author is grateful to all of them.

References

[1] BRAHMS Collaboration: I Arsene *et al*, *Nucl. Phys. A* **757**, 1 (2005)
PHOBOS Collaboration: B B Back *et al*, *Nucl. Phys. A* **757**, 28 (2005)
STAR Collaboration: J Adams *et al*, *Nucl. Phys. A* **757**, 102 (2005)
PHENIX Collaboration: K Adcox *et al*, *Nucl. Phys. A* **757**, 184 (2005)
[2] L D McLerran and T Toimela, *Phys. Rev. D* **31**, 545 (1985)
[3] C Gale and J I Kapusta, *Nucl. Phys. B* **357**, 65 (1991)
[4] H A Weldon, *Phys. Rev. D* **42**, 2384 (1990)
[5] R Rapp and J Wambach, *Adv. Nucl. Phys.* **25**, 1 (2000)
[6] J Alam, S Raha and B Sinha, *Phys. Rep.* **273**, 243 (1996)
[7] J Alam, S Sarkar, P Roy, T Hatsuda and B Sinha, *Ann. Phys.* **286**, 159 (2001)
[8] U Heinz and R Snelling, *Ann. Rev. Nucl. Part. Sci.* **63**, 123 (2013)
[9] P Huovinen and P V Ruuskanen, *Ann. Rev. Nucl. Part. Sci.* **56**, 163 (2006)
[10] T Hirano, arXiv:0808.2684 [nucl-th]
[11] D A Teaney, arXiv:0905.2433 [nucl-th]
[12] P Mohanty, J K Nayak, J Alam and S K Das, *Phys. Rev. C* **82**, 034901 (2010)
[13] P Mohanty, V Roy, S Ghosh, S K Das, B Mohanty, S Sarkar, J Alam and A K Chaudhuri, *Phys. Rev. C* **85**, 031903 (2012)
[14] R Chatterjee, D K Srivastava, U W Heinz and C Gale, *Phys. Rev. C* **75**, 054909 (2007)
[15] R Chatterjee, E S Frodermann, U W Heinz and D K Srivastava, *Phys. Rev. Lett.* **96**, 202302 (2006)
[16] J Deng, Q Wang, N Xu and P Zhuang, *Phys. Lett. B* **701**, 581 (2011)
[17] J F Ownes, *Rev. Mod. Phys.* **59**, 465 (1987)
[18] S D Drell and T-M Yan, *Phys. Rev. Lett.* **25**, 316 (1970)
[19] I R Kenyon, *Rep. Prog. Phys.* **45**, 1261 (1982)
[20] P Aurenche, J Ph Guillet, E Pilon, M Werlen and M Fontannaz, *Phys. Rev. D* **73**, 094007 (2006)
L E Gordon and W Vogelsang, *Phys. Rev. D* **48**, 3136 (1993)
[21] S Gavin, P L McGaughey, P V Ruuskanen and R Vogt, *Phys. Rev. D* **54**, 2606 (1996)
[22] H van Hees and R Rapp, arXiv:0706.4443 [hep-ph]
[23] J Kapusta, P Lichard and D Seibert, *Phys. Rev. D* **44**, 2774 (1991)
[24] R Bair, H Nakkagawa, A Niegawa and K Redlich, *Z. Phys. C* **53**, 433 (1992)
[25] E Braaten and R D Pisarski, *Nucl. Phys. B* **337**, 569 (1990); *ibid*. **339**, 310 (1990)
[26] P Aurenche, F Gelis, R Kobes and H Zaraket, *Phys. Rev. D* **58**, 085003 (1998)
[27] P Arnold, G D Moore and L G Yaffe, *J. High Energy Phys.* **0111**, 057 (2001)
P Arnold, G D Moore and L G Yaffe, *J. High Energy Phys.* **0112**, 009 (2001)
P Arnold, G D Moore and L G Yaffe, *J. High Energy Phys.* **0206**, 030 (2002)

[28] O Kaczmarek and F Zantow, *Phys. Rev. D* **71**, 114510 (2005)
[29] S Sarkar, J Alam, P Roy, A K Dutt-Mazumder, B Dutta-Roy and B Sinha, *Nucl. Phys. A* **634**, 206 (1998)
[30] P Roy, S Sarkar, J Alam and B Sinha, *Nucl. Phys. A* **653**, 277 (1999)
[31] J Alam, P Roy and S Sarkar, *Phys. Rev. C* **71**, 059802 (2005)
[32] K L Haglin, *J. Phys. G* **30**, L27 (2004)
[33] S Turbide, R Rapp and C Gale, *Phys. Rev. C* **69**, 014903 (2004)
[34] NA60 Collaborations: R Arnaldi *et al*, *Phys. Rev. Lett.* **100**, 022302 (2008)
[35] PHENIX Collaboration: A Adare *et al*, *Phys. Rev. C* **81**, 034911 (2010)
[36] J Cleymans, J Fingberg and K Redlich, *Phys. Rev. D* **35**, 2153 (1987)
[37] E Braaten, R D Pisarski and T C Yuan, *Phys. Rev. Lett.* **64**, 2242 (1991)
[38] P Aurenche, F Gelis, G D Moore and H Zaraket, *J. High Energy Phys.* **12**, 006 (2002)
[39] F Karsch, E Laermann, P Petreczky, S Stickan and I Wetzorke, *Phys. Lett. B* **530**, 147 (2002)
[40] O Kaczmarek, E Laermann, M Müller, F Karsch, H-T Ding, S Mukherjee, A Francis and W Soeldner, arXiv:1301.7436 [hep-lat]
[41] S Ghosh, S Sarkar and J Alam, *Eur. Phys. J. C* **71**, 176 (2011)
[42] S Ghosh, S Mallik and S Sarkar, *Eur. Phys. J. C* **70**, 251 (2010)
[43] V L Eletsky, M Belkacem, P J Ellis and J I Kapusta, *Phys. Rev. C* **64**, 035202 (2001)
[44] R A Schneider and W Weise, *Phys. Lett. B* **515**, 89 (2001)
[45] E V Shuryak, *Rev. Mod. Phys.* **65**, 1 (1993)
[46] P Lichard and J Jura, *Phys. Rev. D* **76**, 094030 (2007)
[47] J D Bjorken, *Phys. Rev. D* **27**, 140 (1983)
[48] H von Gersdorff, M Kataja, L D McLerran and P V Ruskanen, *Phys. Rev. D* **34**, 794 (1986)
[49] A K Chaudhuri, arXiv:1207.7028 [nucl-th]
[50] R C Hwa and K Kajantie, *Phys. Rev. D* **32**, 1109 (1985)
[51] D Kharzeev and M Nardi, *Phys. Lett. B* **507**, 121 (2001)
[52] C Bernard *et al*, *Phys. Rev. D* **75**, 094505 (2007)
[53] B Mohanty and J Alam, *Phys. Rev. C* **68**, 064903 (2003)
[54] T Hirano and K Tsuda, *Phys. Rev. C* **66**, 054905 (2002)
[55] F Michler, H Van Hees, D D Dietrich, S Leupold and C Greiner, *Ann. Phys.* **336**, 331 (2013)
[56] C Y Wong, *Introduction to high energy heavy ion collisions* (World Scientific, Singapore, 1994)
[57] J Alam, D K Srivastava, B Sinha and D N Basu, *Phys. Rev. D* **48**, 1117 (1993)
[58] ALICE Collaboration: N Arbor, *EPJ Web Conf.* **60**, 13011 (2013)
[59] WA98 Collaboration: M M Aggarwal, *Phys. Rev. Lett.* **85**, 3595 (2000)
[60] S Mitra, P Mohanty, S Ghosh, S Srakar and J Alam, arXiv:1303.0675
[61] J Alam, S Sarkar, T Hatsuda, T K Nayak and B Sinha, *Phys. Rev. C* **63**, 021901(R) (2001)
D K Srivastava and B Sinha, *Phys. Rev. C* **64**, 034901 (2001)
P Huovinen, P V Ruuskanen and S S Rasanen, *Phys. Lett. B* **535**, 109 (2002)
[62] J Alam, J K Nayak, P Roy, A K Dutt-Mazumder and B Sinha, *J. Phys. G* **34**, 871 (2007)
D d'Enterria and D Peressounko, *Eur. Phys. J. C* **46**, 451 (2006)
[63] PHENIX Collaboration: A Adare *et al*, *Phys. Rev. Lett.* **104**, 132301 (2010)
[64] G Vujanovic, C Young, B Schenke, S Jeon, R Rapp and C Gale, *Nucl. Phys. A* **904–905**, 557c (2013)
[65] T Renk and J Ruppert, *Phys. Rev. C* **77**, 024907 (2008)
[66] C Shen and U Heinz, *Phys. Rev. C* **89**, 044910 (2014)
[67] R Vogt, B V Jacak, P L Mcgaughey and P V Ruuskanen, *Phys. Rev. D* **49**, 3345 (1994)
[68] P Huovinen, P F Kolb, U Heinz, P V Ruuskanen and S A Voloshin, *Phys. Lett. B* **503**, 58 (2001)
[69] H van Hess and R Rapp, *J. Phys. G* **35**, 054001 (2008)

[70] J K Nayak, J Alam, T Hirano, S Sarkar and B Sinha, *Phys. Rev. C* **85**, 064906 (2012)
[71] H van Hees and R Rapp, *Nucl. Phys. A* **806**, 339 (2008)
[72] S Borsanyi *et al*, *J. High Energy Phys.* **11**, 077 (2010)
[73] V Roy and A K Choudhuri, *Phys. Lett. B* **703**, 313 (2011)
[74] ALICE Collaboration: K Aamodt *et al*, *Phys. Rev. Lett.* **106**, 032301 (2011); *Phys. Lett. B* **696**, 30 (2011)
[75] STAR Collaboration: B I Abeleb *et al*, *Phys. Rev. Lett.* **98**, 192301 (2007)
[76] PHENIX Collaboration: S S Adler *et al*, *Phys. Rev. Lett.* **96**, 032301 (2006)
[77] ALICE Collaboration: A Rossi, *Quark matter* (Annecy, France, 23–28 May 2011)
[78] H van Hees, M Mannarelli, V Greco and R Rapp, *Phys. Rev. Lett.* **100**, 192301 (2008)
[79] C M Ko and W Liu, *Nucl. Phys. A* **783**, 23c (2007)
[80] A Adil and I Vitev, *Phys. Lett. B* **649**, 139 (2007)
[81] P B Gossiaux and J Aichelin, *Phys. Rev. C* **78**, 014904 (2008)
[82] S Wicks, W Horowitz, M Djordjevic and M Gyulassy, *Nucl. Phys. A* **784**, 426 (2007)
[83] S Chakraborty and D Syam, *Lett. Nuovo Cimento* **41**, 381 (1984)
[84] B Svetitsky, *Phys. Rev. D* **37**, 2484 (1988)
[85] S K Das, F Scardina and V Greco, arXiv:1312.6857 [nucl-th]
[86] S Mazumder, T Bhattacharyya and J Alam, *Phys. Rev. D* **89**, 014002 (2014)
[87] R Rapp and H van Hees, *Quark gluon plasma* edited by R C Hwa and X-N Wang (World Scientific, 2010) Vol. 4, p. 111
[88] S K Das, J Alam and P Mohanty, *Phys. Rev. C* **82**, 014908 (2010)
S Majumdar, T Bhattacharyya, J Alam and S K Das, *Phys. Rev. C* **84**, 044901 (2012)
[89] M G Mustafa, D Pal and D K Srivastava, *Phys. Rev. C* **57**, 889 (1998)
[90] M L Mangano, P Nason and G Ridolfi, *Nucl. Phys. B* **373**, 295 (1992)
[91] C Peterson *et al*, *Phys. Rev. D* **27**, 105 (1983)
[92] R J Fries, B Mueller and D K Srivastava, *Phys. Rev. Lett.* **90**, 132301 (2003)
[93] G E Brown and M Rho, *Phys. Rev. Lett.* **66**, 2720 (1991)
[94] M Chiu, T K Hemmick, V Khachatryan, A Leonodov, J Liao and L McLerran, arXiv:1202.3679
[95] B Friman, C Höhne, J Knoll, S Leupold, J Randrup, R Rapp and P Senger (Eds.), The CBM physics book, in *Lecture notes in physics* (Springer, 2011) Vol. 814
[96] H Gervais and S Jeon, *Phys. Rev. C* **86**, 034904 (2012)